PCCP

Cite this: *Phys. Chem. Chem. Phys.*, 2011, **13**, 18880–18886

www.rsc.org/pccp

PAPER

Formation of ultracold Rb_2 molecules in the $v'' = 0$ level of the $a^3\Sigma_u^+$ state *via* blue-detuned photoassociation to the $1^3\Pi_g$ state†

M. A. Bellos,*[a] D. Rahmlow,[a] R. Carollo,[a] J. Banerjee,[a] O. Dulieu,[b] A. Gerdes,[c] E. E. Eyler,[a] P. L. Gould[a] and W. C. Stwalley[a]

Received 2nd May 2011, Accepted 17th August 2011
DOI: 10.1039/c1cp21383k

We report on the observation of blue-detuned photoassociation in Rb_2, in which vibrational levels are energetically above the corresponding excited atomic asymptote. ^{85}Rb atoms in a MOT were photoassociated at short internuclear distance to levels of the $1^3\Pi_g$ state at a rate of approximately 5×10^4 molecules s^{-1}. We have observed most of the predicted vibrational levels for all four spin–orbit components; 0_g^+, 0_g^-, 1_g, and 2_g, including levels of the 0_g^+ outer well. These molecules decay to the metastable $a^3\Sigma_u^+$ state, some preferentially to the $v'' = 0$ level, as we have observed for photoassociation to the $v' = 8$ level of the 1_g component.

1 Introduction

Photoassociation (PA) of ultracold atoms is a powerful spectroscopic technique to produce and study ultracold molecules.[1,2] Most photoassociation experiments access vibrational levels that are red-detuned from atomic transitions. Blue-detuned PA, where vibrational levels are energetically above their corresponding atomic asymptote, was first proposed to probe quasibound states[3] and form ultracold Rb_2[4] and KRb molecules.[5] Blue-detuned photoassociation was first observed[6] in our laboratory; however, molecular assignments have remained elusive due to relatively small signals. Blue-detuned photoassociation has also been observed using an intense femtosecond laser,[7] which simultaneously drove resonant and non-resonant transitions to a variety of states, making molecular assignments difficult to perform.

There are two cases where blue-detuned photoassociation could occur: (1) in a local minimum of a potential energy curve repulsive at long range (as in the case here with the $1^3\Pi_g$ state of Rb_2) or (2) in a well that contains a potential barrier and vibrational levels above the atomic asymptote (for instance the $2^1\Sigma_g^+$ state in Rb_2).[8] Although there is no fundamental difference between blue-detuned and red-detuned photoassociation, blue-detuned photoassociation generally occurs at small internuclear distances where the Franck–Condon factors for photoassociation are smaller. Furthermore blue-detuned photoassociation rates may be reduced by optical shielding effects[9] where colliding atoms are prevented from reaching small internuclear distances. However an estimate based on ref. 10 indicates that these effects should be negligibly small for our experimental configuration.

Here, we demonstrate blue-detuned photoassociation to the short-range $1^3\Pi_g$ state of $^{85}Rb_2$ as shown in Fig. 1. This is the first time a free-bound transition to the quasibound $1^3\Pi_g$ state has been directly observed. The $1^3\Pi_g$ state has been previously observed through transitions in heat pipe ovens[4,5,11] and on liquid helium droplets.[12] Photoassociation at short internuclear distance for red-detunings has also been demonstrated[13,14] on the $B^1\Pi$ state of LiCs, yielding ground rovibrational $X^1\Sigma^+$ state molecules.[15] In both these cases, the relatively high efficiency of the photoassociation process at short range is somewhat surprising.

The production of ultracold Rb_2 in the $v'' = 0$, $J'' = 0$ level of the $a^3\Sigma_u^+$ state has previously been achieved[18] through the technique of magnetoassociation followed by STIRAP transfer. The present paper demonstrates a complementary way to reach the same level. The main advantage of the pathway that we demonstrate is experimental simplicity, as it proceeds through a simple PA step followed by spontaneous emission. A distribution of vibrational levels is created in the $a^3\Sigma_u^+$ state, with, in some cases, a significant proportion in the lowest one. A notable difference between the two techniques is that magnetoassociation typically requires temperatures on the order of 100 nK (close to quantum degeneracy), while photoassociation can occur at higher temperatures, such as in magneto-optical traps with temperatures on the order of 100 μK. Also, photoassociation followed by spontaneous emission is irreversible and can provide continuous accumulation of molecules.

2 The $1^3\Pi_g$ potential energy curves

The spin–orbit coupling of the $1^3\Pi_g$ state with neighboring molecular states that correlate to the same asymptotic limit

[a] *Department of Physics, University of Connecticut, Storrs, Connecticut 06269-3046, USA. E-mail: bellos@phys.uconn.edu*
[b] *Laboratoire Aimé Cotton, CNRS, Université Paris-Sud, bât. 505, 91405 Orsay, France*
[c] *Computing and Storage Services, Regional Computer Centre for Lower Saxony, Leibniz Universität, Hannover, Germany*

† Electronic supplementary information (ESI) available: 0_g^+, 0_g^-, 1_g, and 2_g potential energy curves. See DOI: 10.1039/c1cp21383k

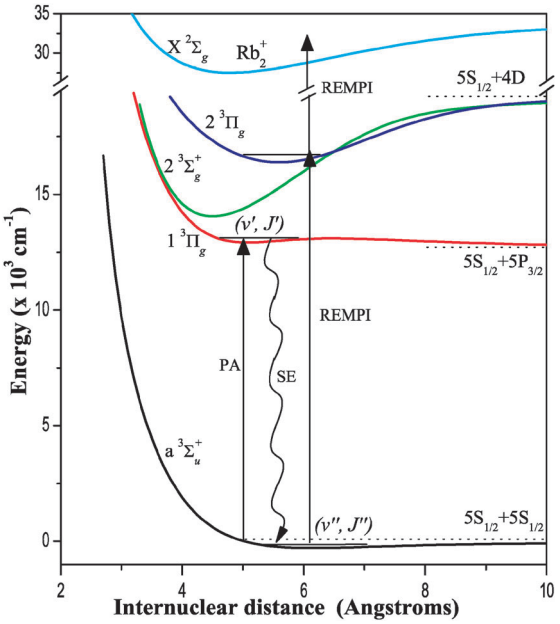

Fig. 1 Scheme for producing and detecting ultracold metastable Rb_2 molecules. Blue-detuned photoassociation (PA) from free atoms to bound levels (v', J') of the $1^3\Pi_g$ state is followed by spontaneous emission (SE) to a variety of (v'', J'') levels of the $a^3\Sigma_u^+$ state. Molecule detection through resonantly enhanced multiphoton ionization (REMPI) is a two step process achieved by first exciting molecules to an intermediate state ($2^3\Sigma_g^+$ or $2^3\Pi_g$), immediately followed by photoionization to produce Rb_2^+. The horizontal dotted lines indicate the positions of atomic asymptotes. The potential energy curves for Rb_2 and Rb_2^+ are from ref. 16 and 17, respectively.

results in four distinct components, $1^3\Pi_g(\Omega = 0^+)$, $1^3\Pi_g(0^-)$, $1^3\Pi_g(1)$, and $1^3\Pi_g(2)$. Where the integer in parenthesis, Ω, is the projection of the total electronic angular momentum on the internuclear axis, g is the parity of the electronic wavefunction by reflection through the center of mass, and ($\pm$) is the symmetry of the electronic wavefunction by reflection through a plane containing the internuclear axis. These states can be expressed more compactly as 0_g^+, 0_g^-, 1_g, and 2_g using Hund's case (c) notation. Their potential energy curves and bound levels are plotted in Fig. 2.

These potential curves are calculated using a rotation-based diabatization method within a quasidegenerate perturbation theory.[19] The sixteen lowest adiabatic states of each relevant symmetry $^3\Pi_g$, $^1\Pi_g$, $^3\Sigma_g^+$, $^1\Sigma_g^+$ in Hund's case (a) are obtained by the method described in ref. 20. This method is based on a representation of the Rb^+ ionic cores by an effective core potential including scalar relativistic terms and core polarization. The electronic Hamiltonian of the related effective two-electron system is expressed in a large basis set of Gaussian orbitals. A full configuration interaction leads to adiabatic potential curves for each relevant molecular symmetry labeled in Hund's case (a). Following ref. 19, the corresponding eigenstates are used as reference states at the internuclear distance of 40 a.u. (1 a.u. = 0.527177 Å), which are considered as representative of the separated-atom states with a reasonable accuracy. At this distance the potential energies including spin–orbit interaction are obtained after diagonalizing the Hamiltonian $H_{so}^{adia} = H^{adia} + H_{so}$, where the diagonal H^{adia} matrix contains the adiabatic energies for all four symmetries

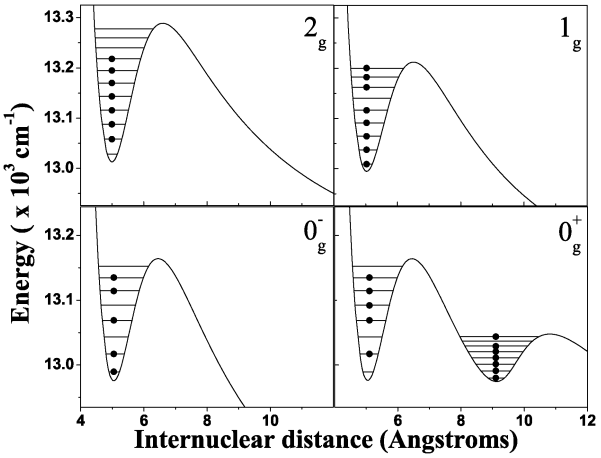

Fig. 2 $1^3\Pi_g$ potential energy curves with spin–orbit coupling, along with vibrational levels calculated by the LEVEL 8.0 program.[21] Dots (•) denote the experimentally observed vibrational levels. The levels that were unobserved most likely have a weaker photoassociation rate, due to low Franck–Condon factor overlaps. The 0_g^+ and 0_g^- states are double well systems, with an inner and outer well. The outer well of the 0_g^- state[22,23] (not shown) occurs at large internuclear distance and is red-detuned from the atomic asymptote.

above, and the coupling matrix H_{so} the relevant atomic spin–orbit coupling terms for the dissociation limits up to $5^2S + 6^2P$.

At each internuclear distance R between 5 a.u. and 40 a.u., a rotation $\mathscr{R}$ of the subspace generated by the sixteen lowest adiabatic states is defined in order to maximize their overlap with the reference states above. This defines an effective Hamiltonian H^{eff} in an atomic-like basis, in which we introduce the H_{so} matrix elements to set up a Hamiltonian matrix H_{so}^{eff}. The diagonalization of H_{so}^{eff} at each R yields potential curves including R-dependent spin–orbit couplings, such as those shown in Fig. 2. Moreover, the inverse rotation $\mathscr{R}^{-1}$ of H_{so}^{eff} back to the initial adiabatic states results in a non-diagonal matrix H_{so}^{diab}, where diagonal elements are the initial adiabatic potential curves, and off-diagonal terms are the R-dependent spin–orbit couplings between these states. This R-dependence is induced by the variation of the admixture of electronic states with internuclear distance. As noted in ref. 19, the efficiency of the model is mainly limited by the overlap of the adiabatic states at R with the reference states, which decreases from unity (at R = 40 a.u. in the present case) to about 70% at R = 10 a.u. As demonstrated in Section 4, these results represent a good basis for the interpretation of the experimental measurements.

3 Experiment

The setup consists of an ^{85}Rb magneto-optical trap (MOT) holding $\sim 10^6$ atoms at a temperature of ~ 125 μK with a density of $\sim 10^{11}$ atoms per cm^3. The MOT trapping laser is locked 14 MHz below the $|5S_{1/2}, F = 3\rangle \rightarrow |5P_{3/2}, F' = 4\rangle$ transition at 780 nm. A repump laser locked on resonance with the $|5S_{1/2}, F = 2\rangle \rightarrow |5P_{3/2}, F' = 3\rangle$ transition is used to pump atoms that spontaneously decay to the $|5S_{1/2}, F = 2\rangle$ state back to the $|5S_{1/2}, F = 3\rangle$ state. Since our optical repumping is not perfect, the energy splitting between the two hyperfine states $|5S_{1/2}, F = 2\rangle$ and $|5S_{1/2}, F = 3\rangle$ of 0.1012 cm^{-1} is one

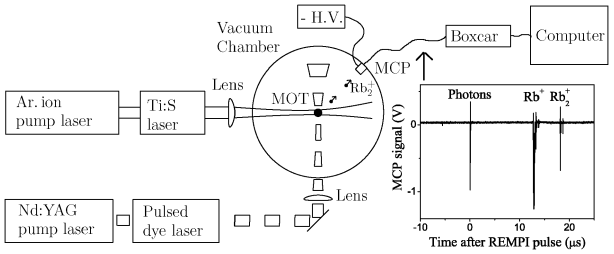

Fig. 3 Schematic diagram of the photoassociation, REMPI and detection systems. The inset shows the time of flight of photons, atomic ions, and molecular ions reaching the MCP detector.

that routinely appears in our PA spectra in the form of weak "hyperfine ghost" lines. We were not able to fully eliminate these atomic "hyperfine ghost" lines from the spectra even after double checking for proper repump laser operation. A tunable cw Ti:sapphire laser (Coherent 899-29) with a power of $\sim$700 mW and a linewidth of 500 kHz is focused approximately to the size of the MOT ($\sim$1 mm diameter) to photoassociate atoms into molecules as shown in Fig. 3. The REMPI laser is a nanosecond pulsed dye laser (Continuum ND6000) with a pulse energy of $\sim$5 mJ and a linewidth of $\sim$0.5 cm^{-1} pumped by a Nd:YAG laser running at 532 nm with a 10 Hz repetition rate. The REMPI laser ionizes the atoms and molecules into Rb^+ and Rb_2^+, respectively. A boxcar averager integrates the ion signal within the time of flight range of Rb_2^+ ions. Our attempts to detect photoassociation by trap loss spectroscopy were unsuccessful; any decrease in MOT fluorescence was smaller than the fluorescence noise of the MOT.

4 Photoassociation spectroscopy

PA spectra were obtained by scanning the PA laser while monitoring the production of Rb_2^+ formed by the REMPI laser. Typical photoassociation spectra are shown in Fig. 4–7. Each spectrum shows rotational lines, atomic "hyperfine ghost" lines, and in some cases molecular hyperfine lines.

If $\Omega > 0$, the electronic angular momentum can couple with the nuclear angular momentum, resulting in molecular hyperfine splittings. Hyperfine splittings are therefore expected for the 2_g and 1_g states, but not for the 0_g^+ and 0_g^- states. We were able to resolve the molecular hyperfine splitting for the 2_g states as shown in the inset of Fig. 4, but were unable to resolve the molecular hyperfine splitting for the 1_g states (inset of Fig. 5) as the splittings are smaller than the observed linewidths.

The PA spectra show rotational lines up to a maximum of $J' = 6$, indicating the presence of s, p, d, and f partial waves in the collision of atoms.[2] This number of partial waves is consistent with the red-detuned PA spectra observed with the same setup. One notable difference is that for red-detuned photoassociation, lines with $J' = 0$, 1, 2, and 3 (arising from s and d partial waves) are stronger than lines with $J' = 4$, 5, and 6 (arising from d and f partial waves), while for blue-detuned photoassociation, lines with $J' = 4$, 5, and 6 are generally stronger than lines with $J' = 0$, 1, 2, and 3. The prevalence of high partial waves in blue-detuned PA could potentially be explained by some kind of heating process. We have ruled out an increase in steady-state temperature of the atoms caused by

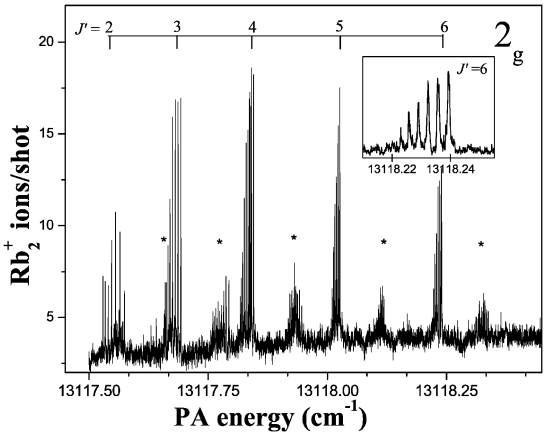

Fig. 4 PA spectrum of the 2_g $v' = 2$ level. The inset shows a closeup of the $J' = 6$ line showing molecular hyperfine structure. Rotational assignments are shown above the spectrum. Lines marked by an (*) are atomic "hyperfine ghost" lines occurring 0.1 cm^{-1} above each rotational line.

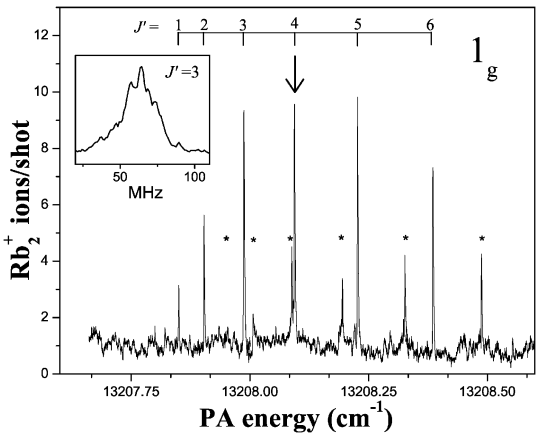

Fig. 5 PA spectrum of the 1_g $v' = 8$ level. Rotational assignments are shown above the spectrum. The arrow (↓) indicates where the PA laser is fixed for the subsequent $a^3\Sigma_u^+$ $v'' = 0$ REMPI spectrum. The inset shows a closeup of the $J' = 3$ line where the molecular hyperfine lines are mostly unresolved. Lines marked by an (*) are atomic "hyperfine ghost" lines occurring 0.1 cm^{-1} above each rotational line.

the blue-detuned PA light, as the ballistic expansion with blue or red-detuned PA light is identical to the ballistic expansion without PA light. We suspect that the change in partial wave distribution between red and blue-detuned PA could be due to flux enhancement effects[24,25] created by the MOT light.

The energy of a rovibrational level is given to the first order by $E_{v,J} = T_v + B_v[J(J+1) - \Omega^2]$. Here T_v and B_v are the term energy and the rotational constant of a vibrational level, respectively. J is the rotational quantum number, which is always greater than or equal to Ω. We extract the experimental rotational constant B_v^{EXP} by fitting a straight line to the energy of the rotational lines *versus* $J(J+1) - \Omega^2$, the results of which are tabulated in Table 1. This fitting process also allowed us to assign an Ω quantum number to each spectrum. The experimental term energies T_v^{EXP} are simply the wavenumbers of the photoassociation laser plus the average thermal energy of collisions ($\sim 10^{-4}$ cm^{-1}). The theoretical rotational constant B_v^{THE} and term energy T_v^{THE} are derived from the *ab initio* potential

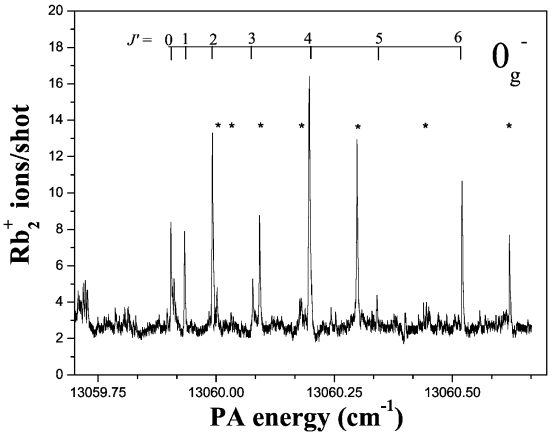

Fig. 6 PA spectra of the 0_g^- $v' = 3$ level. Rotational assignments are shown above the spectra. Lines marked by an (*) are atomic "hyperfine ghost" lines occurring 0.1 cm^{-1} above each rotational line.

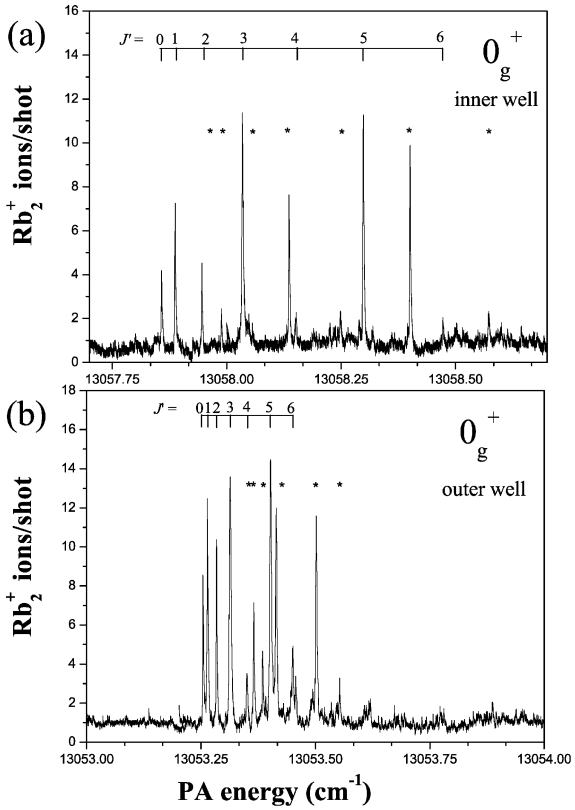

Fig. 7 PA spectra of the 0_g^+ inner well $v' = 3$ level (a) and the 0_g^+ outer well $v' = 5$ level (b). Rotational assignments are shown above the spectra. Lines marked by an (*) are atomic "hyperfine ghost" lines occurring 0.1 cm^{-1} above each rotational line.

energy curves using the LEVEL 8.0 program.[21] Assigning the vibrational quantum numbers to the spectra was greatly simplified by knowledge of the theoretical vibrational energy spacings. After assigning the vibrational numbers, we were able to determine the energy shift to the potential curves necessary make them match the experiment. These energy shifts were −61, −27, −61, −51, and −100 cm^{-1} for the 0_g^+, 0_g^+ outer well, 0_g^-, 1_g, and 2_g states, respectively. The unshifted potential energy curves can be found in ESI.†

Table 1 Experimental and theoretical rotational constants (B_v) and vibrational term energies for $J' = 3$ ($T_{v,\,J'=3}$) for levels of the $1^3\Pi_g$ state in units of cm^{-1}. The theoretical term energies are shifted (see text) to match the experimental term energy of the lowest observed vibrational level. The area (A) under PA spectral lines for $J' = 3$ of the 2_g, 1_g, and 0_g^+ states, and $J' = 4$ of the 0_g^- state in arbitrary units. This line area is an approximation of relative photoassociation rates

State	v'	B_v^{EXP}	B_v^{THE}	$T_{v,J'=3}^{EXP}$	$T_{v,J'=3}^{THE}$	A
2_g	0	—	0.01583	—	13029.293	—
	1	0.0152(9)	0.01568	13059.43(1)	13059.433	1.5
	2	0.01513(3)	0.01550	13089.04(1)	13088.595	1.0
	3	0.0156(3)	0.01530	13117.68(1)	13117.029	14
	4	0.0152(3)	0.01510	13145.44(1)	13144.457	1.1
	5	0.01470(1)	0.01488	13172.06(1)	13170.650	13
	6	0.0143(2)	0.01461	13197.47(1)	13195.609	1.2
	7	0.01382(8)	0.01431	13221.54(1)	13219.201	15
	8	—	0.01395	—	13241.166	—
	9	—	0.01349	—	13261.174	—
	10	—	0.01278	—	13278.579	—
1_g	0	0.0158(2)	0.01561	13008.610(1)	13008.610	8.6
	1	0.0154(2)	0.01543	13037.791(1)	13037.044	1.7
	2	0.01533(3)	0.01523	13065.957(1)	13064.479	14
	3	0.01494(6)	0.01500	13093.040(1)	13090.810	0.8
	4	0.0147(2)	0.01475	13119.053(1)	13115.910	7.2
	5	—	0.01446	—	13139.627	—
	6	0.01423(1)	0.01411	13166.936(1)	13161.752	14
	7	0.01370(2)	0.01366	13188.488(1)	13181.949	0.7
	8	0.01338(6)	0.01299	13207.987(1)	13199.580	4.8
0_g^-	0	0.0151(3)	0.015490	12980.840(1)	12980.840	1.9
	1	0.01507(3)	0.015288	13008.388(1)	13008.264	8.0
	2	—	0.015062	—	13034.674	—
	3	0.01465(5)	0.014816	13060.092(1)	13059.846	7.5
	4	—	0.014534	—	13083.558	—
	5	0.01408(2)	0.014187	13106.164(1)	13105.664	9.4
	6	0.01367(6)	0.013742	13126.527(1)	13125.874	3.6
	7	—	0.013070	—	13143.518	—
0_g^+ inner well	0	—	0.015489	—	12979.282	—
	1	0.01510(3)	0.015286	13006.693(1)	13006.693	5.3
	2	—	0.015058	—	13033.079	—
	3	0.01465(2)	0.014812	13058.035(1)	13058.223	10
	4	0.0141(1)	0.014530	13081.793(1)	13081.910	1.9
	5	0.01396(5)	0.014182	13104.167(1)	13103.983	7.0
	6	0.01364(9)	0.013733	13124.408(1)	13124.144	2.2
	7	—	0.013049	—	13141.709	—
0_g^+ outer well	0	0.00478(8)	0.004791	13005.612(1)	13005.612	0.8
	1	0.00463(8)	0.004828	13016.113(1)	13016.556	0.3
	2	0.00478(5)	0.004851	13026.170(1)	13026.942	4.0
	3	0.00463(7)	0.004859	13035.708(1)	13036.788	12
	4	0.00481(2)	0.004851	13044.764(1)	13046.068	5.1
	5	0.00504(9)	0.004818	13053.313(1)	13054.730	18
	6	—	0.004745	—	13062.674	—
	7	0.00472(2)	0.004561	13068.586(1)	13069.629	6.5

The areas under specific rovibrational lines of the $1^3\Pi_g$ state are also listed in Table 1. This area is proportional to the product of the photoassociation rate and the ionization rate, the latter of which depends on the frequency of the REMPI laser. After varying the REMPI frequency for many of the PA scans in an effort to obtain the strongest Rb_2^+ signal, we expect the reported line areas to roughly approximate the photoassociation rate. If one compares the calculated[4] photoassociation rate to the 0_g^+ outer well with these measured line areas, one can see similarities; namely, an increase in PA rate with vibrational levels followed by strong oscillations.

The lifetimes of levels of the $1^3\Pi_g$ state can be reduced by tunneling through the potential barrier. This tunneling corresponds to a molecule dissociating into two free atoms, and is more likely to happen for higher vibrational levels

Table 2 Energy splitting between ($v' = 1$, $J' = 3$) levels for various states. The theoretical splitting is derived from the potential curves given in the ESI.† The experimental splitting is derived from Table 1

Splitting	Splitting type	Theory/ cm^{-1}	Experiment/ cm^{-1}
2_g–1_g	Spin–orbit	70.1	21.64(1)
1_g–0_g^-	Spin–orbit	19.2	29.403(1)
0_g^+ inner well–0_g^+ outer well	Well position	26.7	−9.420(1)
0_g^-–0_g^+ inner well	Reflection symmetry	−0.5	1.695(1)

where the barrier is less high and narrower. The tunneling lifetime has been calculated for the analogous state in KRb[26] (the $2^3\Pi$ state) and varies between quasi-infinite lifetimes for the $v' = 0$ level and 4×10^{-12} s for the uppermost vibrational level. For Rb_2, the calculated lifetime for the uppermost level of the 0_g^+ outer well[3] is 0.054 ns. This lifetime corresponds to a linewidth of 2950 MHz. So far we have not been able to observe strong broadening of the higher vibrational levels. In particular, we measure a total linewidth for the $v' = 7$ level of the 0_g^+ outer well of less than 50 MHz, and for the $v' = 8$ level of the 1_g state, less than 25 MHz.

The quality of the present theoretical model for molecular spin–orbit can be assessed by looking at the energy shift of potential curves reported above, and the energy splitting between potential curves listed in Table 2. In the internuclear distance range of the inner wells, the potential curves resulting from the diagonalization of H_{so}^{diab} are very similar to the $1^3\Pi_g$ adiabatic one (*i.e.* the diagonal element of H^{adia}), which thus appears to be split into four different spin–orbit components. First of all, it is well known that this kind of quantum chemistry calculation usually predicts potential well depths like the one of the $1^3\Pi_g$ curve with an accuracy of about 100 cm^{-1}. The shifts reported above are thus consistent with this accuracy. The shifts are not the same for all curves, as they involve different Hund's case (*a*) curves with various individual accuracies: the 0_g^+, 0_g^-, and 1_g curves result from the coupling between $^3\Pi_g$ and $^1\Sigma_g^+$, between $^3\Pi_g$ and $^3\Sigma_g^+$, between $^3\Pi_g$, $^1\Pi_g$ and $^3\Sigma_g^+$, respectively, while the 2_g curve involves only $^3\Pi_g$. Nevertheless, it is encouraging that the inner wells of all the states must be shifted by about the same amount to match the position of the experimental levels as described in Table 1. Due to the form of H_{so},‡ the potential well of the 1_g curve is almost unshifted compared to the one of the original $1^3\Pi_g$ curve, as the shift of −51 cm^{-1} (the smallest among inner wells) illustrates. The shift is different for the inner and outer wells of the 0_g^+ curve, which is expected as the spin–orbit model is more accurate for large internuclear distances. The spin–orbit splitting between 1_g and 2_g curves (*i.e.* the spin–orbit coupling diagonal matrix element in H_{so}^{diab} for the 2_g symmetry) is overestimated by about 49 cm^{-1}. In contrast, that for the 0_g^+ and 0_g^- symmetries is underestimated by 10 cm^{-1}. Finally, the tiny splitting between the 0_g^+ and 0_g^- curves can only be predicted, at best, to the right order of magnitude. This is not surprising, as that energy splitting is much smaller than other energy splittings and beyond the accuracy of the present spin–orbit model.

‡ The expressions of the H_{so} matrix for states correlated to an $^2S + {}^2P$ dissociation limit are displayed for instance in ref. 27, and those for the $^2S + {}^2D$ case in ref. 16.

5 REMPI spectroscopy

Molecules in the $1^3\Pi_g$ state spontaneously decay predominantly to the $a^3\Sigma_u^+$ state. Spontaneous decay to the ground electronic state $X^1\Sigma_g^+$ is forbidden due to the electric dipole (E1) selection rules for spin ($\Delta S = 0$) and parity (u → g). The distribution of vibrational levels as a result of spontaneous decay can be approximated by the Franck–Condon factors connecting a single vibrational level of an upper state to a variety of vibrational levels of a lower state.

The Franck–Condon factors (FCFs) for spontaneous emission from 1_g to $a^3\Sigma_u^+$ are shown in Fig. 8; the largest FCF = 0.37 is between the $v' = 8$ and $v'' = 0$ levels. Therefore ~37% of the molecules in the $v' = 8$ level should decay to the $v'' = 0$ level, ~31% to all other vibrational levels $v'' = 1$ to $v'' = 39$, and the remaining ~32% to bound-free transitions that produce free atoms. The FCF's for emission from the 2_g, 0_g^-, and 0_g^+ inner well to the $a^3\Sigma_u^+$ state all have a similar distribution to the one plotted in Fig. 8. The highest FCF from 2_g levels to $v'' = 0$ is 30% starting from the $v' = 9$ level. The highest FCF from the 0_g^+ inner well and 0_g^- levels is 40% starting from the $v' = 7$ level. The 0_g^+ outer well decays almost entirely between the $v'' = 15$ and $v'' = 30$ levels, regardless of the starting vibrational level v'.

To produce a REMPI spectrum, we set the PA laser frequency on a chosen rovibrational level and scan the REMPI laser. With the PA laser set to the 1_g ($v' = 8$, $J' = 4$) level, we obtain a REMPI spectrum (Fig. 9) which shows that $v'' = 0$ is present with a larger population than any other vibrational levels, as predicted by FCF's. Since the initial $a^3\Sigma_u^+$ state population is mostly in a single vibrational level, the REMPI spectrum is simplified and displays mostly the structure of the intermediate states ($2^3\Sigma_u^+$ and $2^3\Pi_g$) rather than a combination of initial ($a^3\Sigma_u^+$) and intermediate states.

The theoretical energies of REMPI transitions are calculated using the term energy of the $a^3\Sigma_u^+$ $v'' = 0$ level and the term energies of the intermediate states. The term energy of the $a^3\Sigma_u^+$ $v'' = 0$ level is calculated to be −234.73 cm^{-1} using

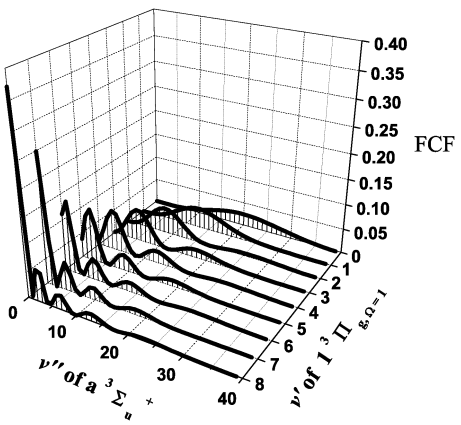

Fig. 8 Franck–Condon factors for spontaneous emission between the $1^3\Pi_{g,\ \Omega=1}$ and $a^3\Sigma_u^+$ states. These calculations from LEVEL 8.0 are based on the 1_g potential presented here and the $a^3\Sigma_u^+$ potential.[28]

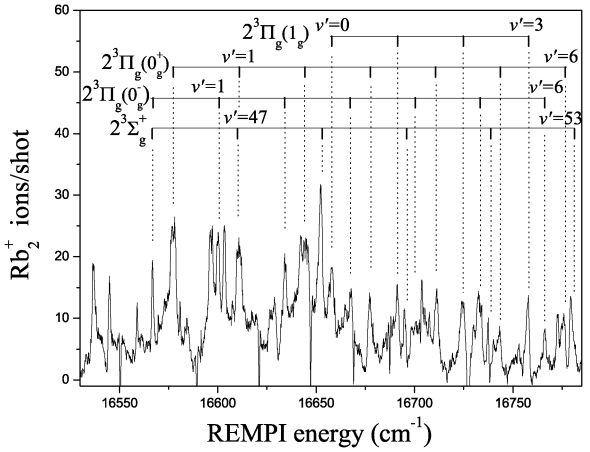

Fig. 9 REMPI spectrum with the PA laser frequency tuned to the ($v' = 8$, $J' = 4$) level of the 1_g state. Tick marks above the spectrum are theoretical transition energies between the $a^3\Sigma_u^+$ $v'' = 0$ level and excited intermediate states $2^3\Sigma_g^+$ and $2^3\Pi_g(0_g^+, 0_g^-, 1_g)$. These transitions account for most of the observed lines.

LEVEL 8.0 and the experimental $a^3\Sigma_u^+$ potential.[28] The term energies of the intermediate states are calculated using LEVEL 8.0 and *ab initio* potentials[8] offset to match experimental data.[16]

6 Transition rates

The PA laser creates molecules in the $1^3\Pi_g$ state, but these quickly decay to the $a^3\Sigma_u^+$ state where their lifetimes are orders of magnitude larger. The radiative lifetime of the $1^3\Pi_g$ state is $\sim$20 ns, while that of the $a^3\Sigma_u^+$ state is estimated[29] to be on the order of 100 s. The lifetime of the $a^3\Sigma_u^+$ state, however, is not limited here by radiative decay but instead by the amount of time the molecules reside in the REMPI beam before dropping ballistically ($\tau_{transit} \approx 5$ ms). Since there are at any given moment orders of magnitude more molecules in the $a^3\Sigma_u^+$ state than in the $1^3\Pi_g$ state, the former state dominates the ionization process. The measured number of Rb_2^+ ions is given by,

$$N_{Rb_2^+} = N_{a^3\Sigma_u^+} p_{ionization} e_d \qquad (1)$$

where $N_{Rb_2^+}$ is the number of Rb_2^+ ions measured per REMPI pulse, $N_{a^3\Sigma_u^+}$ is the steady state number of molecules in rovibrational levels of the $a^3\Sigma_u^+$ state that are resonant with the REMPI laser, $p_{ionization}$ is the photoionization probability per REMPI pulse, and e_d is the efficiency of the ion detector.

Several rovibrational levels of the $a^3\Sigma_u^+$ state could be simultaneously resonant with different intermediate states whereby each would contribute to the total ion signal. However in the case of photoassociation to the $v' = 8$ level of the 1_g state, only the $v'' = 0$ level contributes significantly to the ion signal.

Generally the first step of the REMPI process (bound–bound excitation) is fully saturated by the intense pulsed laser; however the second step of the REMPI process (bound-free photoionization) is not saturated and has a lower probability. We can calculate this ionization probability per pulse from,

$$p_{ionization} = 1 - e^{Wt} = 1 - e^{\frac{\sigma F}{t}t} = 1 - e^{\sigma E\lambda/(hc\pi w^2)} \qquad (2)$$

where the transition rate per second ($W = \frac{\sigma F}{t}$) is given by the photoionization cross section (σ) and the flux (F) per unit time. The flux ($F = E\lambda/(hc\pi w^2)$) is a measure of the total number of photons per unit area. E, λ, and w are the pulse energy, wavelength and the Gaussian beam radius of the REMPI beam. h and c are Planck's constant and the speed of light. Although there are no known photoionization cross sections for the detection scheme we used, we can roughly estimate the cross section to be $\sigma = 1^{+5}_{-0.5} \times 10^{-18}$ cm^2 based on other measurements.[30,31]

Taking for example the transition to the ($v' = 8$, $J' = 4$) level of the 1_g state, we observe $N_{Rb_2^+} = 20$ molecules per REMPI pulse. With the following set of parameters ($\sigma = 1^{+5}_{-0.5} \times 10^{-18}$ cm^2, $E = 5$ mJ, $\lambda = 600$ nm, $w = 1.4$ mm, $N_{Rb_2^+} = 20$, and assuming $e_d = 1$) we obtain $N_{a^3\Sigma_u^+} = 90^{+80}_{-60}$ molecules residing within the REMPI beam volume in the steady state.

Solving the rate equation for the number of $a^3\Sigma_u^+$ state molecules, we obtain

$$N_{a^3\Sigma_u^+}(t) = \frac{R_{PA}\,FCF\,t}{1 + t/\tau} \qquad (3)$$

where R_{PA} is the photoassociation rate per second, τ is the transit time lifetime of $a^3\Sigma_u^+$ molecules and FCF is the fraction of $1^3\Pi_g$ molecules that decay to a particular vibrational level of the $a^3\Sigma_u^+$ state. For the typical parameter values of FCF = 0.37 and $\tau_{transit} = 5$ ms, we obtain a photoassociation rate of $R_{PA} = 5^{+4}_{-1.5} \times 10^4$ molecules per second.

7 Conclusions

We have observed the formation of ultracold Rb_2 molecules in the $v'' = 0$ level of the $a^3\Sigma_u^+$ state. The molecules are formed *via* blue-detuned photoassociation of the $1^3\Pi_g$ state as proposed in ref. 4. We have performed spectroscopy of the $1^3\Pi_g$ state and found good agreement with *ab initio* potentials. We have shown that the 1_g $v' = 8$ level decays mainly to the $a^3\Sigma_u^+$ $v'' = 0$ level. We expect equivalent schemes for photoassociation and ground state production to work for other alkali dimers. For instance, K_2[3] and several heteronuclear alkali dimers[32] have blue detuned wells at short internuclear distance, in a situation analogous to the one for Rb_2.

Acknowledgements

We gratefully acknowledge support from the NSF, AFOSR, and the UConn Research Foundation. A.G. acknowledges support from the Research Training Group 665 "Quantum interference and applications" Germany and from Laboratoire Aimé Cotton. Enlightening discussions with Johannes Deiglmayr and Fernand Spiegelman about the diabatization procedure are gratefully acknowledged.

References

1 W. C. Stwalley and H. Wang, *J. Mol. Spectrosc.*, 1999, **195**, 194–228.
2 K. M. Jones, E. Tiesinga, P. D. Lett and P. S. Julienne, *Rev. Mod. Phys.*, 2006, **78**, 483–535.
3 O. Dulieu, R. Kosloff, F. Masnou-Seeuws and G. Pichler, *J. Chem. Phys.*, 1997, **107**, 10633–10642.

4 M.-L. Almazor, O. Dulieu, F. Masnou-Seeuws, R. Beuc and G. Pichler, *Eur. Phys. J. D*, 2001, **15**, 355–363.
5 H. Skenderović, R. Beuc, T. Ban and G. Pichler, *Eur. Phys. J. D*, 2002, **19**, 49–56.
6 M. Pichler, J. Qi, W. C. Stwalley, R. Beuc and G. Pichler, *Phys. Rev. A: At., Mol., Opt. Phys.*, 2006, **73**, 021403.
7 F. Weise, A. Merli, F. Eimer, S. Birkner, F. Sauer, L. Wöste, A. Lindinger, W. Salzmann, T. G. Mullins, R. Wester, M. Weidemüller, R. Aganoglu and C. P. Koch, *J. Phys. B: At., Mol. Opt. Phys.*, 2009, **42**, 215307.
8 S. J. Park, S. W. Suh, Y. S. Lee and G.-H. Jeung, *J. Mol. Spectrosc.*, 2001, **207**, 129–135.
9 L. Marcassa, S. Muniz, E. de Queiroz, S. Zilio, V. Bagnato, J. Weiner, P. S. Julienne and K. A. Suominen, *Phys. Rev. Lett.*, 1994, **73**, 1911–1914.
10 V. Sanchez-Villicana, S. D. Gensemer, K. Y. N. Tan, A. Kumarakrishnan, T. P. Dinneen, W. Süptitz and P. L. Gould, *Phys. Rev. Lett.*, 1995, **74**, 4619–4622.
11 D. Veža, R. Beuc, S. Milosević and G. Pichler, *Eur. Phys. J. D*, 1998, **2**, 45–52.
12 M. Mudrich, P. Heister, T. Hippler, C. Giese, O. Dulieu and F. Stienkemeier, *Phys. Rev. A: At., Mol., Opt. Phys.*, 2009, **80**, 042512.
13 J. Deiglmayr, P. Pellegrini, A. Grochola, M. Repp, R. Côté, O. Dulieu, R. Wester and M. Weidemüller, *New J. Phys.*, 2009, **11**, 055034.
14 J. Deiglmayr, P. Pellegrini, A. Grochola, M. Repp, R. Côté, O. Dulieu, R. Wester and M. Weidemüller, *New J. Phys.*, 2010, **12**, 079802.
15 J. Deiglmayr, A. Grochola, M. Repp, K. Mörtlbauer, C. Glück, J. Lange, O. Dulieu, R. Wester and M. Weidemüller, *Phys. Rev. Lett.*, 2008, **101**, 133004.
16 J. Lozeille, A. Fioretti, C. Gabbanini, Y. Huang, H. K. Pechkis, D. Wang, P. L. Gould, E. E. Eyler, W. C. Stwalley, M. Aymar and O. Dulieu, *Eur. Phys. J. D*, 2006, **39**, 261–269.
17 A. Jraij, A. Allouche, M. Korek and M. Aubert-Frécon, *Chem. Phys.*, 2003, **290**, 129–136.
18 F. Lang, K. Winkler, C. Strauss, R. Grimm and J. H. Denschlag, *Phys. Rev. Lett.*, 2008, **101**, 133005.
19 R. Cimiraglia, J. P. Malrieu, M. Persico and F. Spiegelmann, *J. Phys. B: At. Mol. Phys.*, 1985, **18**, 3073.
20 M. Aymar and O. Dulieu, *J. Chem. Phys.*, 2005, **122**, 204302.
21 R. J. Le Roy, *LEVEL 8.0: A Computer Program for Solving the Radial Schrödinger Equation for Bound and Quasibound Levels*, University of Waterloo Chemical Physics Research Report CP-663, 2007.
22 R. A. Cline, J. D. Miller and D. J. Heinzen, *Phys. Rev. Lett.*, 1994, **73**, 632–635.
23 C. Amiot, *Chem. Phys. Lett.*, 1995, **241**, 133.
24 V. Sanchez-Villicana, S. D. Gensemer and P. L. Gould, *Phys. Rev. A: At., Mol., Opt. Phys.*, 1996, **54**, R3730–R3733.
25 A. Fioretti, D. Comparat, C. Drag, T. F. Gallagher and P. Pillet, *Phys. Rev. Lett.*, 1999, **82**, 1839–1842.
26 J. T. Kim, D. Wang, E. E. Eyler, P. L. Gould and W. C. Stwalley, *New J. Phys.*, 2009, **11**, 055020.
27 R. Beuc, M. Movre, V. Horvatic, C. Vadla, O. Dulieu and M. Aymar, *Phys. Rev. A: At., Mol., Opt. Phys.*, 2007, **75**, 032512.
28 C. Strauss, T. Takekoshi, F. Lang, K. Winkler, R. Grimm, J. Hecker Denschlag and E. Tiemann, *Phys. Rev. A: At., Mol., Opt. Phys.*, 2010, **82**, 052514.
29 S. J. J. M. F. Kokkelmans, H. M. J. Vissers and B. J. Verhaar, *Phys. Rev. A: At., Mol., Opt. Phys.*, 2001, **63**, 031601.
30 H. Suemitsu and J. A. R. Samson, *Phys. Rev. A: At., Mol., Opt. Phys.*, 1983, **28**, 2752–2758.
31 D. M. Creek and G. V. Marr, *J. Quant. Spectrosc. Radiat. Transfer*, 1968, **8**, 1431–1436.
32 W. C. Stwalley, J. Banerjee, M. Bellos, R. Carollo, M. Recore and M. Mastroianni, *J. Phys. Chem. A*, 2010, **114**, 81–86.

